CHEMISTRY OF MATERIALS
Article

Chem. Mater. **2010,** *22,* 175–185 175
DOI:10.1021/cm902788s

Epitaxial Calcium and Strontium Fluoride Films on Highly Mismatched Oxide and Metal Substrates by MOCVD: Texture and Morphology

Andrey V. Blednov,*,† Oleg Yu. Gorbenko,‡,§ Sergey V. Samoilenkov,⊥ Vadim A. Amelichev,‡ Vasiliy A. Lebedev,† Kirill S. Napolskii,† and Andrey R. Kaul‡

†*Department of Materials Science, and* ‡*Department of Chemistry, Moscow State University, Vorobievy Gory, 1, building 3, 119991 Moscow, Russia, and* ⊥*Institute of High Temperatures, Russian Academy of Sciences, Izhorskaya Street, 13/19, 125412 Moscow, Russia.* §*Deceased on December 12, 2008.*

Received September 7, 2009. Revised Manuscript Received November 13, 2009

The growth of epitaxial CaF_2 and SrF_2 thin films on single crystalline *r*-cut sapphire, MgO (001) and biaxially textured Ni−W polycrystalline tape by low-temperature MOCVD is reported. A novel and efficient combination of alkaline-earth and fluorine precursors was used for deposition. A comprehensive study regarding the out- and in-plane orientation of the films and their surface morphology is presented using X-ray diffraction (XRD), Rutherford backscattering spectroscopy (RBS), energy-dispersive X-ray analysis (EDX), field-emission scanning electron microscopy (FESEM), atomic force microscopy (AFM), and electron backscatter diffraction (EBSD). The grown films are shown to have different crystallographic orientation depending on the film−substrate lattice mismatch and growth rate. Both types of films were obtained with pure *c*-axis orientation on all used substrates by either choosing the appropriate deposition conditions or postdeposition treatment. Epitaxial relations for all grown films are determined. A film−substrate interaction is described for the case of Ni−W substrate; a way to avoid it is proposed and successfully implemented. Certain growth conditions are shown to result in a unique three-dimensional ordered nanogrid structure of the films, making them perfect nanotemplated substrate for the epitaxial growth of other functional layers.

Introduction

Inorganic fluorides have been intensively studied for a long time because they exhibit a number of unique properties that make them perfect materials for a wide range of potential applications, first of all, in optics and electronics.[1,2] Among them, special and very important materials are fluorides of alkaline-earth metals, in particular, CaF_2 and SrF_2. They are dielectric and have a wide transmission range (from mid-infrared to vacuum ultraviolet) and extremely low refractive indices thus being very useful for microelectronic and optoelectronic devices, optical components (such as lenses, windows, prisms), optical coatings, multilayers, efficient optical filters, and waveguides.[3−6] Besides, the structural properties and oxygen resistivity (even at high temperatures) of these compounds make them perfect buffer layer materials used for deposition of different classes of oxides onto semiconductors and other substrates.[7−9] At last, particular attention is paid toward the thin films of ionic insulators on metal surfaces. These systems are attractive for both technological applications such as fabrication of sensors,[10] resonant tunneling devices,[11] magnetic tunnel junctions,[12] and for fundamental studies of different physical phenomena occurring on the metal−insulator interface.[13,14] As one can see, many of these applications require fluorides in the form of good-quality thin films, grown epitaxially on appropriate substrate. However, epitaxial CaF_2 and SrF_2 films were reported only for few single-crystalline substrates having good lattice match with them, mainly Si,[15−17]

*Corresponding author. Tel./Fax: (007) 495 939 14 92. E-mail: blednov@inorg.chem.msu.ru.

(1) Rainer, F.; Lowdermilk, W. H.; Milam, D.; Carniglia, C. K.; Hart, T. T.; Lichtenstein, T. L. *Appl. Opt.* **1985**, *24*, 496.
(2) Mademann, D.; Raupach, L.; Weissbrodt, P.; Hacker, E.; Kaiser, U.; Kaiser, N. *Fresenius J. Anal. Chem.* **1993**, *346*, 173.
(3) Tsai, R. Y.; Shiau, S. C.; Lin, D.; Ho, F. C.; Hua, M. Y. *Appl. Opt.* **1999**, *38*, 5452.
(4) Fujihara, S.; Kadota, Y.; Kimura, T. *J. Sol−Gel Sci. Technol.* **2002**, *24*, 147.
(5) Fork, D. K.; ArmaniLeplingard, F.; Lui, M.; McFarlane, R. A. *J. Lightwave Technol.* **1996**, *14*, 611.
(6) McFarlane, R. A.; Lui, M.; Yap, D. *IEEE J. Sel. Top. Quantum Electron.* **1995**, *1*, 82.
(7) Tiwari, A. N.; Blunier, S.; Zogg, H.; Lerch, P.; Marcenat, F.; Martinoli, P. *J. Appl. Phys.* **1992**, *71*, 5095.
(8) Hung, L. S.; Mason, G. M.; Pazpujalt, G. R.; Agostinelli, J. A.; Mir, J. M.; Lee, S. T.; Blanton, T. N.; Ding, G. *J. Appl. Phys.* **1993**, *74*, 1366.
(9) Moon, B. K.; Ishiwara, H. *Jpn. J. Appl. Phys.* **1994**, *33*, 5911.
(10) Fergus, J. W. *Sens. Actuators B* **1997**, *42*, 119.
(11) Watanabe, M.; Suemasu, T.; Muratake, S.; Asada, M. *Appl. Phys. Lett.* **1993**, *62*, 300.
(12) Kobayashi, K.; Suemasu, T.; Kuwano, N.; Hara, D.; Akinaga, H. *Thin Solid Films* **2007**, *515*, 8254.
(13) Okiji, A.; Kasai, H. *Surf. Sci.* **1979**, *86*, 529.
(14) Kiguchi, M.; Katayama, M.; Yoshikawa, G.; Saiki, K.; Koma, A. *Appl. Surf. Sci.* **2003**, *212−213*, 701.
(15) Farrow, R. F. C.; Sullivan, P. W.; Williams, G. M.; Jones, G. R.; Cameron, D. C. *J. Vac. Sci. Technol.* **1981**, *19*, 415.
(16) Schowalter, L. J.; Fathauer, R. W.; Goehner, R. P.; Turner, L. G.; Deblois, R. W.; Hashimoto, S.; Peng, J. L.; Gibson, W. M.; Krusius, J. P. *J. Appl. Phys.* **1985**, *58*, 302.
(17) Ishiwara, H.; Asano, T. *Appl. Phys. Lett.* **1982**, *40*, 66.

Published on Web 12/08/2009

GaAs,[18,19] InP,[20,21] Ge,[22] and few others, including Cu and Al_2O_3 (for both only CaF_2 films were studied).[23−25] To the best of our knowledge, no epitaxial growth of strontium and/or calcium fluoride films on substrates with big lattice mismatch or polycrystalline substrates has been reported so far.

Among the deposition techniques, the most widely used are physical vapor deposition methods, such as molecular-beam epitaxy (MBE),[15,21,26−30] thermal evaporation,[31−33] pulsed laser deposition (PLD),[34,35] and electron-beam evaporation (EBE).[36,37] In some works, atomic layer deposition (ALD) was employed using separate fluorinating agents like HF[38] or TiF_4.[39]

Metal-organic chemical vapor deposition (MOCVD) possesses several significant advantages over the other deposition techniques. Among them are the simplicity of film and precursor composition control, the high throughput and possibility of depositing films on large-area and curved substrates. In addition, MOCVD allows the separation of precursors from the deposition chamber and does not require any special and expensive equipment. The main problem in depositing alkaline-earth fluoride films by MOCVD is a lack of convenient precursors both for alkaline-earth metals and fluorine. Although successful experiments on MOCVD growth of fluoride films have been reported for all alkaline-earth metals[40,41] using single fluorine-containing precursors,[42] such deposition technique requires high enough partial pressures of oxygen in the reaction atmosphere to prevent significant carbon contamination of the film which is inadmissible in case of oxidation-sensitive substrates (e.g., metals and semiconductors). Besides, the use of simple and cheap separate precursors for alkaline-earth and fluorine seems to be more convenient for large-scale industrial deposition processes because it enables higher deposition rate/throughput and is more cost-efficient.

In this paper, we report on growing epitaxial thin films of Ca and Sr fluorides on different single-crystalline and metallic polycrystalline substrates by MOCVD using modified metal-organic alkaline-earth metal precursor and ammonium hydrogen fluoride as a separate fluorine source. The orientation and surface morphology of the films are extensively studied.

Experimental Section

Substrates. In the present work, three types of substrates were used, namely, single crystals of Al_2O_3 ($1\bar{1}02$) and MgO (001) (hereinafter *r*-sapphire and MgO, respectively), and metal tapes from $Ni_{0.95}W_{0.05}$ alloy (80−100 μm thick) with (00*l*)[*h*00] biaxial texture (evico GmbH, Germany, hereinafter Ni−W).

Precursors. The choice of alkaline-earth metal precursor was a challenging problem. It is widely known that dipivaloylmethanates $M(tmhd)_2$ (M = Ca, Sr, tmhd = 2,2,6,6-tetramethyl-3,5-heptanodionate) usually used as alkali earth precursors tend to saturate their coordination sphere by absorbing water or polymerization,[43,44] thus the use of coordinationally saturated compounds makes sense. Alkaline-earth metal precursors used in this work were the adducts of metal dipivaloylmethanates with bidentate neutral ligand 1,10-phenantroline (Phen), $M(tmhd)_2 \cdot 2Phen$, which are more stable during storage and exhibit better volatility than $M(tmhd)_2$ even for M = Ba.[45,46]

For the metal precursor synthesis, a novel and simple high-yield approach was demonstrated. At first, solid $M(tmhd)_2$ complexes were synthesized according to the standard procedure (by precipitation from $M(NO_3)_2$ and Htmhd (Fluka, Germany) alcohol-aqueous solutions)[47] and purified by sublimation. No absorption lines in the range 3800−3100 cm^{-1} were present in the IR-spectra of the products, i.e., the complexes contained no water. At the next stage, they were dissolved in *p*-xylene with addition of stoichiometric amount of *o*-phenantroline (Chempur, Germany) and the solution was slowly heated to xylene's boiling point (138 °C). During the heating the rest of water was removed from the solution in the form of azeotrope with xylene (40% water, 60% xylene, B.P. 94.5 °C). At last, the solution was cooled to 15 °C, which caused adduct precipitation with a yield of about 90%. Anal. Calcd (found) for $CaC_{46}H_{54}N_4O_4$: C, 72.06 (71.99); H, 7.05 (7.13); N, 7.31 (7.27). Calcd (found) for $SrC_{46}H_{54}N_4O_4$: C, 67.81 (66.66); H, 6.63 (6.82); N, 6.88 (6.71). Some noticeable decrease of measured C and N content and increase of H content with respect to the calculated values was observed for Sr precursor. This is most likely due to slight absorption of water by Sr complex after the first stage of synthesis and further incomplete substitution of water molecules

(18) Siskos, S.; Fontaine, C.; Munozyague, A. *J. Appl. Phys.* **1984**, *56*, 1642.
(19) Rao, V. J.; Chaudhari, G. N. *Appl. Phys. A: Mater. Sci. Process.* **1992**, *54*, 284.
(20) Sinharoy, S.; Hoffman, R. A.; Rieger, J. H.; Warner, J. D.; Bhasin, K. B. *J. Vac. Sci. Technol., A* **1986**, *4*, 897.
(21) Weiss, W.; Kasper, K.; Herrmann, K. H.; Schmeisser, D.; Göpel, W. *Surf. Sci.* **1992**, *268*, 319.
(22) Omori, S.; Ishii, H.; Nihei, Y. *Appl. Surf. Sci.* **1998**, *130*, 67.
(23) Calleja, F.; Hinarejos, J. J.; de Parga, A. L. V.; Suturin, S. M.; Sokolov, N. S.; Miranda, R. *Surf. Sci.* **2005**, *582*, 14.
(24) Barkai, M.; Grünbaum, E.; Deutscher, G. *Vacuum* **1990**, *41*, 847.
(25) Haag, M.; Dabringhaus, H. *J. Cryst. Growth* **1997**, *178*, 298.
(26) Sullivan, P. W.; Farrow, R. F. C.; Jones, G. R. *J. Cryst. Growth* **1982**, *60*, 403.
(27) Schowalter, L. J.; Fathauer, R. W. *J. Vac. Sci. Technol. A* **1986**, *4*, 1026.
(28) Heral, H.; Bernard, L.; Rocher, A.; Fontaine, C.; Munozyague, A. *J. Appl. Phys.* **1987**, *61*, 2410.
(29) Sokolov, N. S.; Suturin, S. M. *Appl. Surf. Sci.* **2001**, *175*, 619.
(30) Pasquali, L.; Suturin, S. M.; Ulin, V. P.; Sokolov, N. S.; Selvaggi, G.; Giglia, A.; Mahne, N.; Pedio, M.; Nannarone, S. *Phys. Rev. B* **2005**, *72*, 045448.
(31) Chaudhari, G. N.; Rao, V. J. *Appl. Phys. Lett.* **1993**, *62*, 852.
(32) Chaudhari, G. N.; Rao, V. J. *Semicond. Sci. Technol.* **1993**, *8*, 412.
(33) Pasquali, L.; D'Addato, S.; Selvaggi, G.; Nannarone, S.; Sokolov, N. S.; Suturin, S. M.; Zogg, H. *Nanotechnology* **2001**, *12*, 403.
(34) Shushtarian, S. S.; Ogale, S. B.; Chaudhari, G. N.; Singh, P.; Rao, V. J. *Mater. Lett.* **1991**, *12*, 335.
(35) Maki, T.; Okamoto, K.; Sugiura, M.; Hosomi, T.; Kobayashi, T. *Appl. Surf. Sci.* **2002**, *197*, 448.
(36) Klust, A.; Kayser, R.; Wollschlager, J. *Phys. Rev. B* **2000**, *62*, 2158.
(37) Kruschwitz, J. D. T.; Pawlewicz, W. T. *Appl. Opt.* **1997**, *36*, 2157.
(38) Ylilammi, M.; Rantaaho, T. *J. Electrochem. Soc.* **1994**, *141*, 1278.
(39) Pilvi, T.; Arstila, K.; Leskela, M.; Ritala, M. *Chem. Mater.* **2007**, *19*, 3387.
(40) Purdy, A. P.; Berry, A. D.; Holm, R. T.; Fatemi, M.; Gaskill, D. K. *Inorg. Chem.* **1989**, *28*, 2799.
(41) Fragalà, M. E.; Toro, R. G.; Rossi, P.; Dapporto, P.; Malandrino, G. *Chem. Mater.* **2009**, *21*, 2062.
(42) Malandrino, G.; Castelli, F.; Fragalà, I. L. *Inorg. Chim. Acta* **1994**, *224*, 203.
(43) Brooks, J.; Davies, H. O.; Leedham, T. J.; Jones, A. C.; Steiner, A. *Chem. Vap. Deposition* **2000**, *6*, 66.
(44) Fromm, K. M.; Gueneau, E. D. *Polyhedron* **2004**, *23*, 1479.
(45) Sato, R.; Takahashi, K.; Yoshino, M.; Kato, H.; Ohshima, S. *Jpn. J. Appl. Phys.* **1993**, *32*, 1590.
(46) Drozdov, A. A.; Troyanov, S. I.; Kuzmina, N. P.; Martynenko, L. I.; Alikhanyan, A. S.; Malkerova, I. P. *J. Phys. IV* **1993**, *3*, 379.
(47) Hammond, G. S.; Nonhebel, D. C.; Chin-Hua, S. W. *Inorg. Chem.* **1963**, *2*, 73.

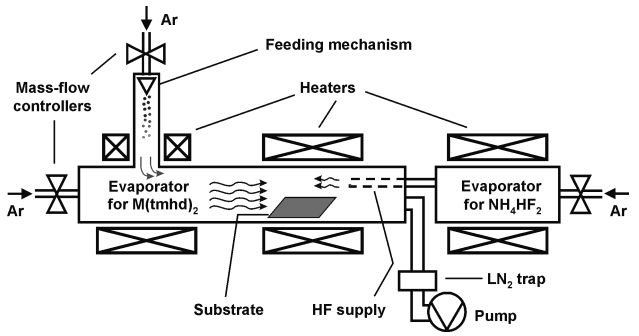

Figure 1. Schematic representation of the MOCVD setup.

by xylene. However, the substitution level for Sr precursor calculated from elemental analysis data is higher than 98%. This small impurity did not affect in any way the volatility of precursor and the composition of resulting films.

Ammonium hydrogen fluoride was used as a separate fluorine source. This precursor is cheap and easily available, solid at room temperature, safe in storage and manipulation, and the amount of HF evolved during its thermal decomposition (at given P_{total} and carrier gas flow velocity) can easily be controlled by changing the decomposition temperature.

MOCVD Experiments. All film depositions were carried out in the original setup made from stainless steel consisting of a hot-wall reactor and two precursor evaporators (Figure 1). During the deposition the pulse vibrational feeding mechanism supplied micro portions of solid metal precursor to the evaporator heated up to 220/240 °C for Ca/Sr precursor, correspondingly (on the early stages of the work this supply system was replaced by a nickel boat with precursor placed in the hot zone of the evaporator). The $M(tmhd)_2$ flow was varied in the range of $6 \times 10^{-9} - 2 \times 10^{-8}$ mol/s. Ammonium hydrogen fluoride was thermally decomposed in a separate evaporator at 60 °C evolving gaseous HF with a constant flow of about 6×10^{-7} mol/s. Preliminary experiments have shown that higher HF flows lead to a very rapid reaction between the precursors and formation of solid MF_2 in the gaseous phase, resulting in a film with poor surface quality.

Chemical reactions occurring in the deposition system are the decomposition of precursors during evaporation (eqs 1 and 2) and the film deposition itself (eq 3):

$$M(tmhd)_2 \cdot 2Phen(s) = M(tmhd)_2(g) + 2Phen(g) \quad (1)$$

$$NH_4HF_2(s) = NH_4F(s) + HF(g) \quad (2)$$

$$M(tmhd)_2(ads) + 2HF(g) = MF_2(s) + 2Htmhd(g) \quad (3)$$

Low deposition temperatures ranging from 250 to 450 °C were tested. Most films were deposited at 400 °C and total pressure of 16−17 mbar, using 99.993% Ar as a carrier gas. The gas flows through the evaporators were adjusted to provide a uniform MF_2 layer thickness along the substrate. No fluorination of the substrates and no oxidation of Ni (up to 400 °C) occurred under these conditions.

Film Characterization. The thickness and composition of obtained films were estimated by RBS using He^+ ions with energy 1.5 MeV and FESEM/EDX (Leo Supra 50 VP/Oxford Instruments INCA Energy+).

The phase composition, crystal structures, out- and in-plane orientations of the films were studied by XRD using Rigaku SmartLab diffractometer with Cu Kα radiation and incident beam Ge (220) × 2 monochromator ($\theta-2\theta$, φ-scanning, grazing incidence ($2\theta\chi-\varphi$) XRD).

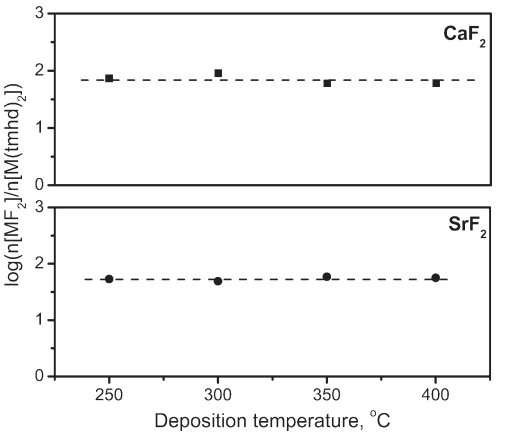

Figure 2. Kinetics of fluoride films deposition: evidence of diffusion-controlled process.

The films' surface morphology and roughness were examined by FESEM and AFM (NT-MDT NTEGRA Aura). Prior to SEM analysis, a thin conductive layer of carbon was sputtered onto films using Edwards Scancoat system. The AFM was operated in tapping mode; for routine measurements, custom silicon cantilevers (MikroMasch) were used, and high-resolution AFM images were obtained using MikroMasch cantilevers with single crystal diamond (SCD) tip. All images were taken in air at room temperature.

To investigate the surface texture of the films, we employed EBSD (Jeol JSM-840A SEM + Oxford Instruments HKL Channel 5).

Results and Discussion

Film Growth Kinetics. The kinetic investigations were performed using a Ni boat as alkaline-earth metal supply system, which exhibited some deviations in the rate of precursor weight loss during different experiments. Although these deviations were not very sufficient we normalized the thickness of every certain film not only to deposition time but also to the amount of precursor evaporated during its deposition in order to get correct and reliable growth rate values. Figure 2 represents the logarithm of ratio $n(MF_2)/n(M(tmhd)_2)$ plotted versus deposition temperature, where $n(MF_2)$ and $n(M(tmhd)_2$ stand for the amounts of fluoride in the film and evaporated precursor, correspondingly. This ratio characterizes the efficiency of precursor use during the deposition and can therefore serve as a direct and convenient characteristic of the film growth rate. Alkaline-earth metal fluoride amount can be estimated from mean film thickness, substrate surface, and material density (assumed to be equal to the bulk density).

Film growth rate turned out to be independent of deposition temperature in the range of 250−400 °C for both Ca and Sr fluorides, which is clear evidence of the diffusion-controlled regime of film growth in these experimental conditions. To explain this, one should take into account that the reaction leading to the film formation (see eq 3) is, in fact, a simple displacement of a weak

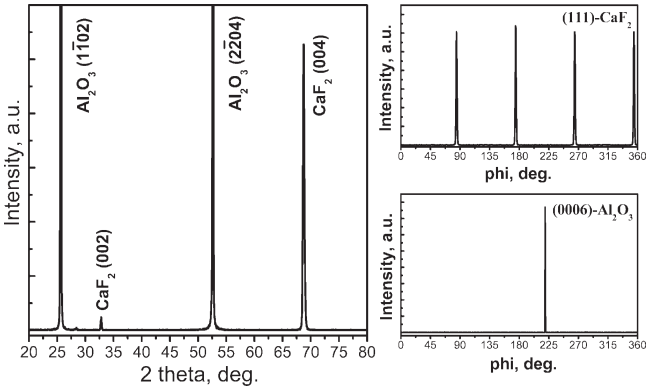

Figure 3. XRD patterns of CaF_2 film on *r*-sapphire. Left: $\theta-2\theta$ scan. Right: φ-scans of (111) CaF_2 and (0006) sapphire reflections.

acid anion by a stronger one. It is an enthalpy-driven process that obviously exhibits weak dependence on the process temperature (its rate is very fast at temperatures studied) and therefore the rate-limiting stage in this case is expected to be diffusion rather than kinetics. In contrast to this, the reaction of the same alkaline-earth precursor with oxygen leading to the formation of oxide film represents a kinetically controlled process, because it involves dissociation of oxygen molecules and destruction of the precursor carbon chain which are comparatively slow temperature dependent processes.[48] Moreover, the counter-flow scheme of precursor delivery implemented in our deposition system implies a cross diffusion of precursor flows, which is an obvious diffusion barrier, possibly determining the diffusion deposition regime.

Film Composition and Thickness. All as-deposited films contained only alkaline-earth metals and fluorine ions. EDX did not reveal any detectable amounts of carbon, oxygen or metals other than alkaline-earth in the films (detection limits are about 1 wt % for C and O and <0.1 wt % for possible metal contaminants−components of the setup material). Additionally, the thin surface layer (10−15 nm) of all films was indexed as MF_2 by EBSD. All these observations allow us to conclude that no detectable contamination of the films occurred during the deposition.

The film thickness estimated from RBS measurements was in the range of 10−800 nm, depending on the precursor supply rate and deposition time. For the films thicker than 200 nm on single-crystalline substrates the RBS data were confirmed by SEM study of the sample cross-section.

Film Texture. All as-deposited films were crystalline, though the crystallinity decreased with decreasing the deposition temperature which resulted in somewhat lower XRD peak intensities. In all cases the most intensive reflections in $\theta-2\theta$ XRD patterns of the films were (*hhh*) and (00*l*), whereas other reflections were absent or of very low intensity. The results of texture studies turned out to be different for *r*-sapphire and MgO/Ni−W substrates. Therefore, they are reported within two separate sections for better clarity.

(48) Zeng, Z.; Natesan, K. *Fusion Eng. Des.* **2004**, *70*, 87.

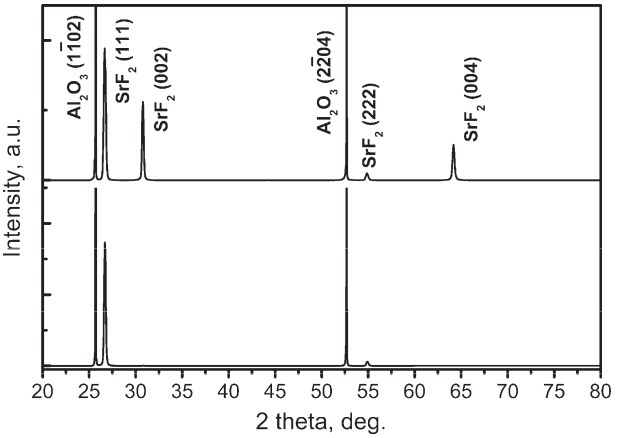

Figure 4. XRD $\theta-2\theta$ patterns of SrF_2 films deposited on *r*-sapphire with low (below) and higher (above) rates.

Films on r-Sapphire. (A) CaF_2 Films on *r*-Sapphire. Fluoride films on *r*-sapphire substrates showed a different orientation depending on the film composition. All deposited CaF_2 films exhibited pure (001) orientation (Figure 3) that was independent of the growth rate and film thickness in the intervals studied. The φ-scan for (111) CaF_2 reflection contains four peaks separated by exactly 90° of rotation angle. It reveals a perfect single type in-plane cubic texture of CaF_2 layer corresponding to the epitaxial relation CaF_2-(001)[100]$\|$ Al_2O_3(1$\bar{1}$02)[11$\bar{2}$0]. The full width at half-maximum (FWHM) of the peaks was found to be $\Delta\varphi = 1.6°$. This value is, at first sight, relatively high as compared to $\Delta\varphi < 0.1°$ for the substrate, but a substantial lattice mismatch between CaF_2 ($a = 5.46$ Å) and sapphire (unit cell in the *r*-plane: 4.76 Å × 5.13 Å) should be taken into account.

(B) SrF_2 Films on *r*-Sapphire. A different situation was observed for SrF_2 films on *r*-sapphire. In this case the slowly grown films (growth rate <1.5 Å/s) were almost purely (111) oriented, whereas (001) orientation appeared in the films grown with higher deposition rates (Figure 4). Purely (001) oriented films were obtained only for very high deposition rates. The explanation of this intriguing phenomenon will be given below, along with the description of surface morphology of differently oriented films. For (111) SrF_2 films on *r*-sapphire the formation of in-plane variant structures was determined by φ-scanning (Figure 5). As seen from Figure 5, four different peak series are observed on the φ-scan, situated ±13.5, ±13.5 ± 60, ±13.5 ± 120, and ±193.5° apart from the substrate peak. They represent the (111) oriented SrF_2 unit cells with their (11$\bar{2}$) axes rotated ±16.5° or ±76.5° with respect to (1$\bar{1}$0$\bar{1}$) axis of sapphire. For such growth illustrated schematically on Figure 6, the following epitaxial relations for out-of-plane and four different in-plane orientations are proposed: SrF_2(111)$\|$ Al_2O_3(1$\bar{1}$02), SrF_2[11$\bar{2}$]$\|$ Al_2O_3[$\bar{2}$02$\bar{1}$], [20$\bar{2}$ $\bar{1}$], [$\bar{2}$20$\bar{1}$], and [$\bar{2}\bar{2}$0$\bar{1}$], respectively. It should be noted that φ-scan peaks have an asymmetric shape (see inset in Figure 5), which most probably results from a slight tilting of the SrF_2 (111) axis normal to the substrate surface. The peaks corresponding to the reflections from the orientation variants (A and B, C and D in Figure 6) have shoulders on their opposite sides. The value of FWHM was the same for all

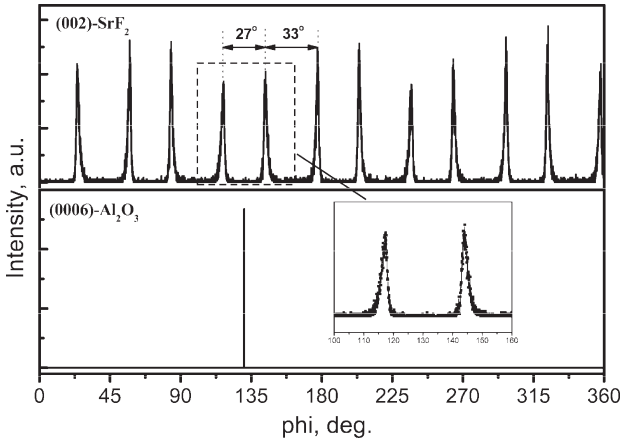

Figure 5. XRD φ-scans of (002) SrF_2 and (0006) sapphire reflections of the (111) oriented SrF_2 film on *r*-sapphire. The peaks have asymmetric profiles, as can clearly be seen in the inset.

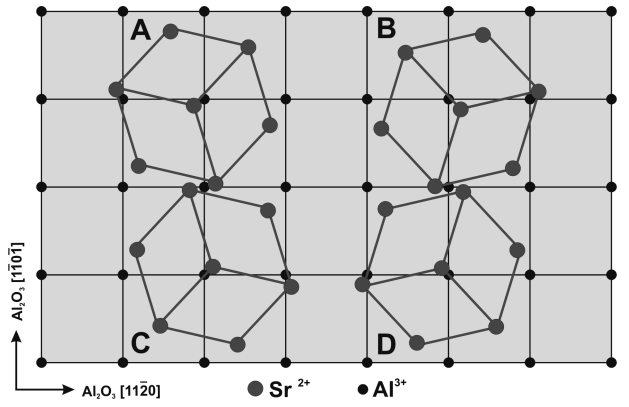

Figure 6. Schematic representation of (111) oriented SrF_2 films growth on *r*-sapphire.

peaks series, with an average $\Delta\varphi = 1.8°$, indicating a good crystal quality of the film.

The φ-scanning of (001) oriented SrF_2 films showed they had a good in-plane texture with epitaxial relations SrF_2-(001)[100]‖ $Al_2O_3(1\bar{1}02)[11\bar{2}0]$ and $\Delta\varphi = 2.3°$ (Figure 7). This value substantially exceeds the one for (001) oriented CaF_2 films because of a higher lattice mismatch between SrF_2 ($a = 5.80$ Å) and *r*-sapphire.

Films on MgO and Ni−W. CaF_2 and SrF_2 films deposited onto MgO substrates exhibited a mixture of orientations, (001) being the dominant one and (111) the main admixture. A similar situation was observed for Ni−W tape substrates: as-deposited fluoride films had a mixed (001) + (111) out-of-plane orientation with minor admixtures of other orientations. In order to obtain the films with pure *c*-axial texture we subjected them to a series of postdeposition recrystallization annealings. They were held in the temperature range 600−900 °C, at total pressures of 3−1000 mbar using different annealing atmospheres (Ar, Ar+5%H_2, Ar+HF). The annealing duration was 1 h. A criterion to determine the optimal annealing conditions was the formation of pure (00*l*) texture of the fluoride. This approach, indeed, led to the uniquely (001) oriented films (Figure 8, shown are the XRD patterns for films on Ni−W substrates only).

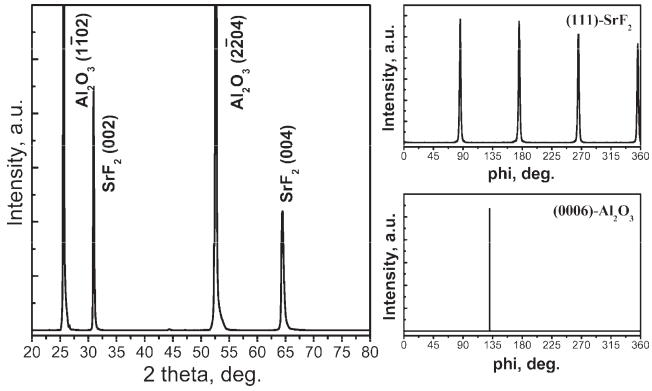

Figure 7. XRD patterns of (001) oriented SrF_2 film on *r*-sapphire. Left: $\theta-2\theta$ scan. Right: φ-scans of (111) SrF_2 and (0006) sapphire reflections.

Optimal annealing temperatures were found to be 700 and 800 °C for CaF_2 and SrF_2 films, respectively. That is in good accordance with the values of Tamman temperatures for these materials (Tamman temperature, $T_t = 0.5-0.8T_M$, where T_M is the melting temperature, characterizes the appearance of effective bulk diffusion in the sample) and significantly lower than temperatures required for crystallization of epitaxial fluorite-structured oxide films (1000 °C and more).[49−51] The reason for that might be the higher diffusive mobility of F^- ion as compared to oxygen ions in oxides. Annealing films at temperatures exceeding optimal ones caused their secondary recrystallization and corruption of the single type of orientation as judged by the appearance of (111) admixture reflections in XRD $\theta-2\theta$ patterns of such films (Figure 8, upper patterns). The influence of annealing atmosphere on film orientation was observed only for films on Ni−W substrates and is described in detail below.

Along with pure out-of-plane *c*-axial texture annealed samples demonstrated the sharp cubic in-plane orientation of the single type, as was revealed by φ-scanning (Figure 9). Epitaxial relations for the fluoride films grown on MgO and Ni−W substrates can be written as (001)[100]‖(001)[100] and (001)[100]‖(001)[110] for CaF_2 and SrF_2, correspondingly (Figure 10, shown are the growth schemes for films on MgO substrates only). It is remarkable that CaF_2 films deposited onto MgO single crystals exhibit much higher FWHM values of φ-scan peaks than SrF_2 on MgO, which indicates sharper in-plane texture of the latter. The explanation for that might be that growth of SrF_2 film on MgO with rotation of the film unit cell by 45° provides a good lattice match already at small size of the coincidence site lattice: 1 rotated SrF_2 unit cell matches well the 2 unit cells of MgO (with acceptable $\Delta = 2.3\%$), whereas for unrotated CaF_2, the

(49) Graboy, I. E.; Markov, N. V.; Maleev, V. V.; Kaul, A. R.; Polyakov, S. N.; Svetchnikov, V. L.; Zandbergen, H. W.; Dahmen, K. H. *J. Alloys Compd.* **1997**, *251*, 318.
(50) Sathyamurthy, S.; Paranthaman, M.; Bhuiyan, M. S.; Payzant, E. A.; Lee, D. F.; Goyal, A.; Li, X.; Kodenkandath, T.; Schoop, U.; Rupich, M. *IEEE Trans. Appl. Supercond.* **2005**, *15*, 2974.
(51) Bhuiyan, M. S.; Paranthaman, M.; Sathyamurthy, S.; Aytug, T.; Kang, S.; Lee, D. F.; Goyal, A.; Payzant, E. A.; Salama, K. *Supercond. Sci. Technol.* **2003**, *16*, 1305.

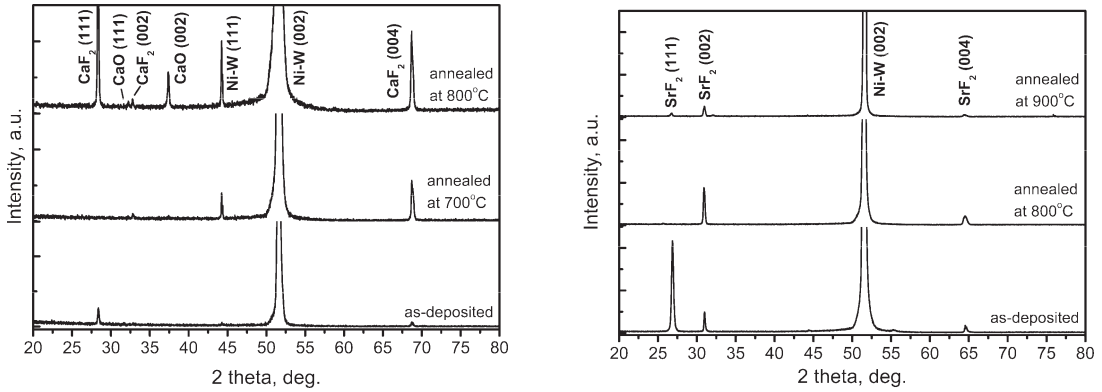

Figure 8. XRD $\theta-2\theta$ patterns of CaF_2 and SrF_2 films deposited on Ni−W substrates and annealed in optimal and nonoptimal conditions.

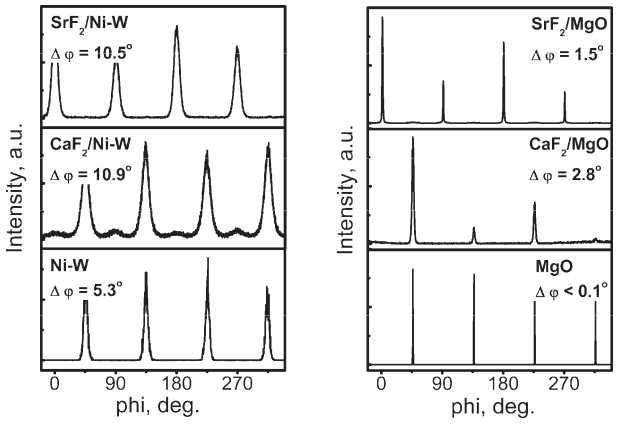

Figure 9. φ-scans for (111) reflections of Ni−W and MgO substrates and CaF_2 and SrF_2 films on them.

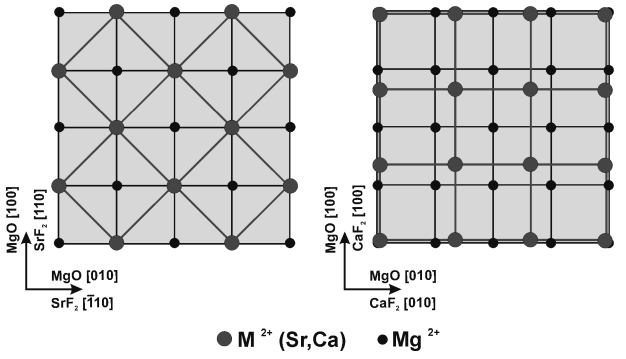

Figure 10. Schematic representation of (001) oriented growth of SrF_2 (left) and CaF_2 (right) films on MgO (001).

similar mismatch is achieved only at ratio 3 CaF_2 to 4 MgO unit cells (Figure 10). Interestingly, the effect of film−substrate mismatch on the quality of epitaxy is much weaker in the films deposited onto Ni−W tapes. The reason for such a difference should be that in this case the film quality is strongly influenced, besides the match of lattice parameters of the film and substrate, by surface imperfection of the latter. Surface roughness and defectiveness of a polycrystalline metal tape is evidently much higher than those of a polished single crystal, thus the influence of match of lattice parameters between the film and substrate is significantly decreased.

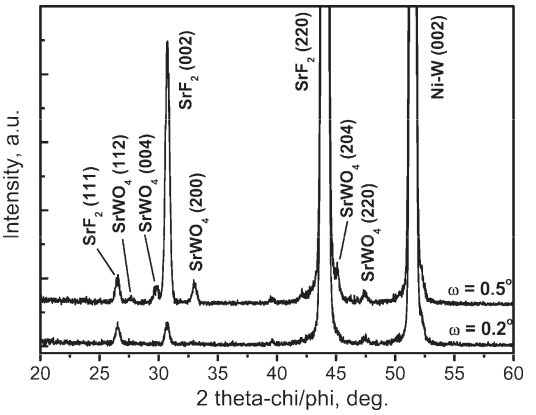

Figure 11. Grazing incidence XRD pattern of SrF_2 film containing $SrWO_4$ on the film−substrate interface. Omega stands for the beam incidence angle. As far as the incident beam is almost parallel to the sample surface, diffraction is seen from planes perpendicular to it, e.g., for (220) instead of (111).

The use of Ni−W tapes as substrates introduced some difficulties in achieving the single cubic orientation in the fluoride films. In the initial experiments with Ar as the annealing gas a partial oxidation of the substrate material occurred during recrystallization annealing and the resulting products reacted chemically with the film material. This process caused the formation of oxygen-containing $CaWO_4$ and $SrWO_4$ phases having a scheelite-type structure. Grazing incidence XRD study of such samples has clearly shown that mixed oxide is formed on the film−substrate interface and is missing in the bulk of film: shown in Figure 11 are the typical patterns for fluoride films indicating that with decreasing the beam incidence angle the intensity of reflections from oxide phase drops to zero (only one peak at $2\theta = 47.5°$ that can be attributed to this phase is present in the pattern recorded at incidence angle of 0.2°. Its intensity is decreased by a factor of 2 as compared to the pattern recorded at 0.5°, confirming the formation of oxide phase on the film−substrate interface rather than in the bulk of film. The presence of this peak in the XRD pattern may result from the large data acquisition area along with relatively high surface roughness of the film which plays an important role in case of grazing incidence study). Besides, we observed the change of film in-plane orientation

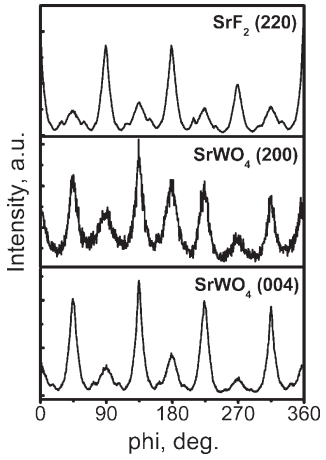

Figure 12. Grazing incidence XRD φ-scans of (004) and (200) reflections of $SrWO_4$ and (220) SrF_2 reflection. The sample studied is a SrF_2 film on Ni−W with $SrWO_4$ admixture on film−substrate interface.

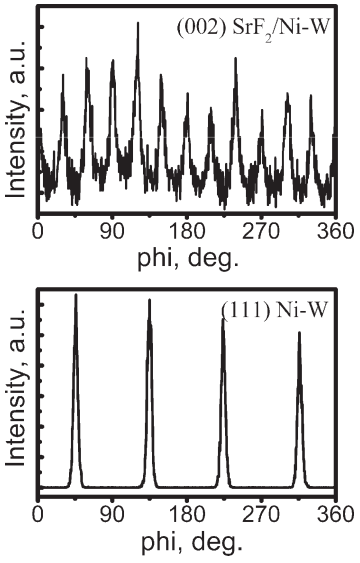

Figure 13. XRD φ-scans of (111) Ni and (002) SrF_2 reflections of thin (111) oriented SrF_2 film on Ni−W.

in samples containing these oxide phases from pure (001)[100]‖(001)[110] for SrF_2 or (001)[100]‖(001)[100] for CaF_2 films to the mixture of these orientations. To explain this phenomenon the in-plane orientation of MWO_4 was studied. Figure 12 represents the grazing incidence XRD φ-scans for (004) and (200) peaks of $SrWO_4$ and (220) peak of SrF_2. It is clearly visible that $SrWO_4$ exhibits the oriented growth on Ni−W with several in-plane orientations and serves as a basis for growth of subsequent SrF_2 layer in the same orientations since the lattice parameters of the two phases match well (5.8 Å for SrF_2 and $a = b = 5.42$ Å, $c/2 = 5.98$ Å for $SrWO_4$). Similar observations were made for CaF_2 films on Ni−W (the corresponding lattice parameters are 5.46 Å for CaF_2 and $a = b = 5.24$ Å, $c/2 = 5.69$ Å for $CaWO_4$). By introducing 5% H_2 to the annealing gas, we managed to successfully suppress the oxidation processes and obtain CaF_2 and SrF_2 films with a single type of in-plane orientation.

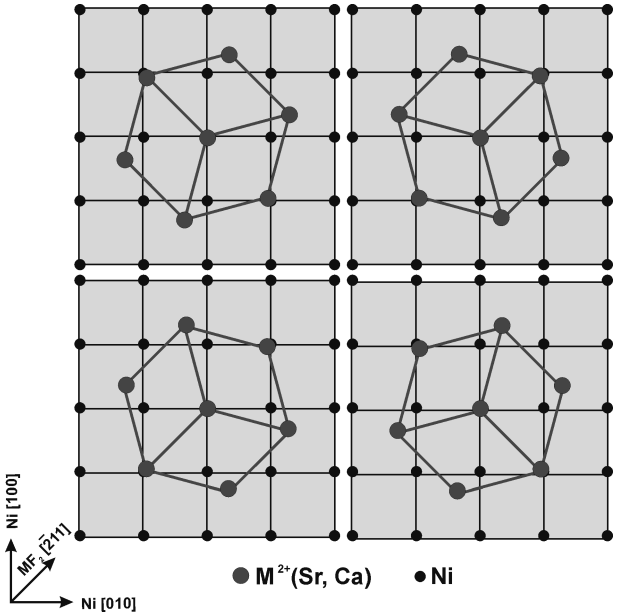

Figure 14. Schematic representation of (111) oriented growth of SrF_2 and CaF_2 films on Ni−W. The indicated $[\bar{2}11]$ MF_2 direction refers to the lower left scheme. On another 3 schemes, the MF_2 unit cell is rotated 90, 180, and 270° in the drawing plane with respective rotation of the $[\bar{2}11]$ vector.

Another observation made on samples on Ni−W substrates was the effect of film thickness on its orientation. All obtained thin (10−30 nm) films of both Ca and Sr fluorides were purely (111) oriented. The φ-scanning revealed that four different equivalent variants of in-plane film orientation are observed (Figure 13, shown is the pattern for SrF_2 film on Ni−W), each φ-scan peak of the film being 15 or 45° apart from the substrate peaks. Such growth is illustrated by a schematic diagram in Figure 14. The corresponding epitaxial relations are $MF_2(111)$‖Ni(100) for out-of-plane orientation, and $MF_2[\bar{2}11]$‖Ni[110], $[1\bar{1}0]$, $[\bar{1}10]$, and $[\bar{1}\,\bar{1}0]$ for 4 in-plane orientation variants. In the case of SrF_2, such growth provides an appropriate mismatch of 4.9%, whereas for CaF_2, it exceeds 10%, resulting in a poorer in-plane orientation (lower intensities and higher FWHM values of φ-scan peaks). In contrast to films thicker than 30 nm that demonstrated mixed type of orientation after the deposition and were recrystallized during the annealing, the pure (111) orientation of the thin ones could not be changed by postdeposition treatment. This can be explained by the fact that no recrystallization can occur if a film is uniformly crystallized with a single type of orientation: in such a case, no crystallites with the other orientation are present that can serve as starting nuclei for the new grains.

Films' Surface. The properties of the film surface play a key role for their practical applicability, especially when a multilayer structure is assembled. Among these properties the most important are the surface texture and morphology: the first one predetermines the possibility of growing the subsequent layer with desired orientation, whereas the second one allows predicting its roughness, which is often a parameter of critical importance.

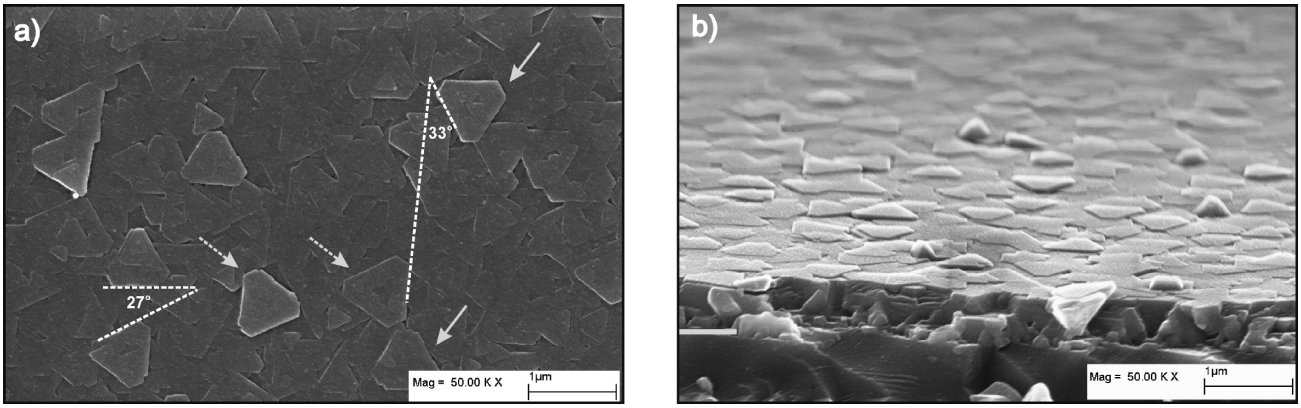

Figure 15. (a) Plane view SEM micrograph of SrF_2 film on *r*-sapphire with pure (111) orientation. Arrowed by solid and dash are the triangles of different orientations and their mirror images. (b) Cross-section micrograph of the same film. Some (001) oriented pyramidal nuclei are present on the background.

Surface Morphologies. The surface morphology of fluoride films depended drastically on their crystallographic orientation, growth rate, and thickness. Figures 15−20 show the different types of film surface morphologies that were observed in our work.

(A) Films with (111) Orientation. In the case of purely (111) oriented film on *r*-sapphire (which were obtained only for SrF_2 at growth rates <1.5 Å/s), it consists of the characteristic flat triangle hillocks (often truncated) of about 8−15 nm in height representing the hexagonal lattice planes (Figures 15a and 16A). The SrF_2 triangles grow in two different in-plane orientations rotated by 27 or 33° with respect to each other (see Figure 5 for comparison). For each orientation, mirror-image triangles are also present, which is in full accordance with the results of XRD φ-scanning that revealed four types of in-plane orientation. This structure is quite typical for (111) growth of alkaline-earth fluorides and was observed also on other nonoxide single crystal substrates.[16,52] The film itself is dense, pore-free (Figure 15b) and rather smooth. The average mean square roughness R_s of such a film does not exceed 6 nm (determined by AFM over a 1×1 μm^2 scan) taking into consideration that the triangles are of finite height and form layered structure. The surface of a single triangle is found to have a very low R_s value of about 2 nm (on a scan 0.3×0.3 μm^2 in size). The reason for that is the low free energy of (111) surface in the fluorite crystal. Its energy value is the lowest among all low-index fluorite crystal surfaces[27,53] and therefore the described crystal shape corresponds to the global energy minimum that can be achieved in this system.

It is also worth noting that some microcracks can be seen in the dense (111) oriented films (Figure 17a) induced by a significant difference in thermal expansion coefficients (TECs) of the film and substrate (TEC values are about 18.5×10^{-6} and 5×10^{-6} K^{-1} at room temperature for SrF_2 and Al_2O_3, respectively[54−56]).

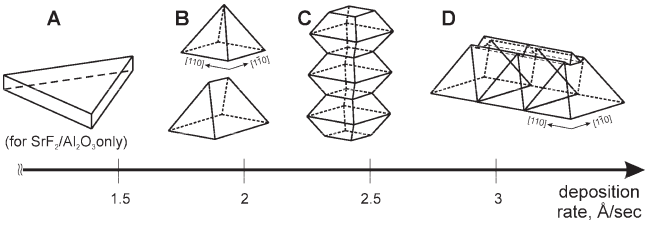

Figure 16. Schematic representation of different types of crystallite shape in the fluoride films.

(B) Films with (001) Orientation. The films in which (001) orientation was present exhibited a totally different morphology that was dependent on the film deposition rate. Here we would like to distinguish between the SrF_2 and CaF_2 films in order to describe our observations and explanations for them in detail.

As mentioned above, the slowly grown SrF_2 films were almost purely (111) oriented, whereas the increase in deposition rate induced the formation of (001) orientation. The surface of these thin mixed (111) + (001) oriented films deposited with rates 1.5−2 Å/s is represented by rectangular or hip rooflike pyramids with their lateral surface formed by (111) facets growing on the top of layer comprised by flat triangles (Figure 16B and 17a). Similar observations were reported for fluoride films on Si.[28,29] The reason for such shape of (001) oriented crystallites is once again the high free energy of (001) surface in the fluorite crystal. Although the numerical energy values are available only for (111) and (110) surfaces, either calculated[57,58] or experimentally measured[59] (both approaches place these values around 5×10^{-5} J/cm^2 for (111) surface and 7×10^{-5} to 1×10^{-4} J/cm^2 for (110)), it is generally admitted that they are much lower than those for (100) surface because the latter has a dipole moment perpendicular to it and therefore its energy is too high for smooth and extensive (001) free surface to be formed. It can theoretically be achieved either in the form of an epitaxial thin film or by reconstruction of the crystal surface. However, in the former case, the (100) surface is not free but is rather situated on the interface of two phases,[27] whereas the latter case seems to be

(52) Fathauer, R. W.; Schowalter, L. J. *Appl. Phys. Lett*. **1984**, *45*, 519.
(53) Tasker, P. W. *J. Phys. Coll*. **1980**, *41*, C6–488.
(54) White, G. K.; Roberts, R. B. *High Temperatures−High Pressures* **1983**, *15*, 321.
(55) Wachtman, J. B., Jr; Scuderi, T. G.; Cleek, G. W. *J. Am. Ceram. Soc*. **1962**, *45*, 319.
(56) Roberts, R. B.; White, G. K. *J. Phys. C: Solid State Phys*. **1986**, *19*, 7167.
(57) Benson, G. C.; Claxton, T. A. *Can. J. Phys*. **1963**, *41*, 1287.
(58) Tasker, P. W. *J. Phys. C: Solid State Phys*. **1979**, *12*, 4977.
(59) Gilman, J. J. *J. Appl. Phys*. **1960**, *31*, 2208.

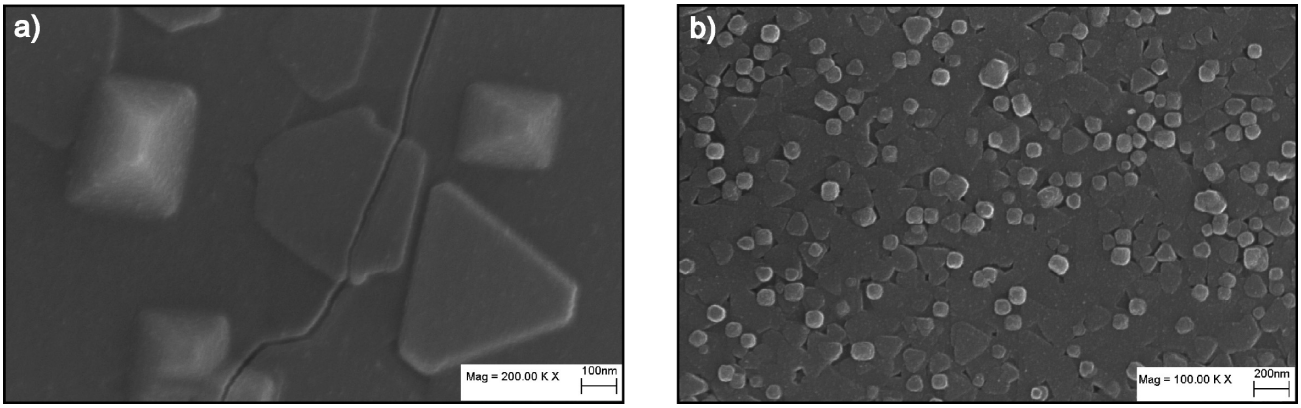

Figure 17. SEM micrographs with different magnification of SrF_2 films on *r*-sapphire with mixed (111)+(001) orientation.

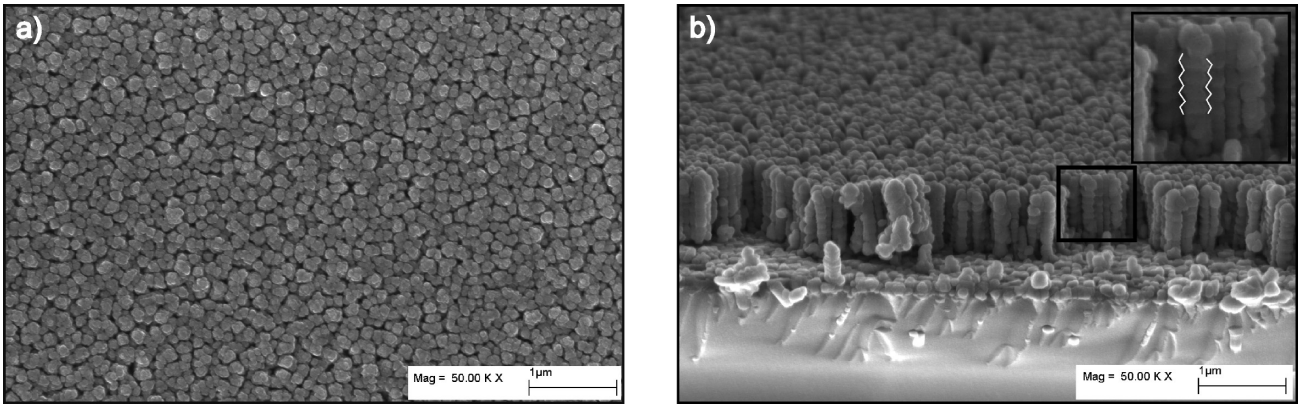

Figure 18. (a) Plane view and (b) cross-section SEM micrographs of SrF_2 film on *r*-sapphire with (001) orientation. The inset in b shows the enlarged image of the selected area with a single column comprised by (111) faceted crystallites.

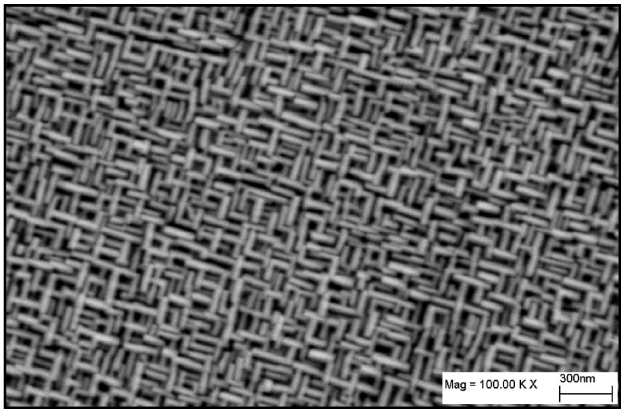

Figure 19. SEM micrograph of rapidly grown SrF_2 film on *r*-sapphire with (001) orientation representing a nanogrid film structure.

not possible in practice[60] except for some special growth modes (e.g., in the presence of water, which can form an electric double layer on crystal surface and serve for a compensation of the dipole moment of the (100) surface).[61]

It is important to notice that the pyramidal crystallites appear on the top of (111) oriented layer and primarily at the joint of (111) oriented SrF_2 crystallites, i.e. in-between the flat and smooth triangles (Figure 17b). We believe it is due to an increased number of crystallization centers in such structure as compared to the initial smooth single crystal surface. The high deposition rate along with availability of a great number of crystallization centers lead to the formation of (001) oriented crystallites instead of (111) oriented. This occurs most likely because of a benefit in the total surface energy: the inner volume (i.e., the quantity of film material) of rectangular-based (111) faceted pyramid is almost twice that of a flat triangle-based prism with the same surface area (the calculation is made for characteristic triangle and pyramid basement sides of 500 and 300 nm, respectively). Besides, the pyramidal crystallite is faceted by (111) planes only, whereas side faces of a triangle prism are (110) planes having a 1.5−2 times higher energy, and this fact enhances the energetic advantage of (001) growth at high deposition rate. In other words, such surface morphology of rapidly grown films corresponds to a local minimum of the surface energy for this system. However, at low deposition rate the surface diffusion of the film components at growth temperature is sufficient to distribute the supplied material over a larger area and to form a dense and flat film: note that for (111) oriented films, very few crystallite boundaries are seen, and furthermore, the height of triangular crystallites is extremely low (8−15 nm). These both facts favor the minimization of surface energy of the "undesired" (110) side faces of a prism and the total surface energy of such a structure seems to be the bare minimum for this particular

(60) Tasker, P. W. *Surf. Sci.* **1979**, *87*, 315.
(61) Deuster, V.; Schick, M.; Kayser, T.; Dabringhaus, H.; Klapper, H.; Wandelt, K. *J. Cryst. Growth* **2003**, *250*, 313.

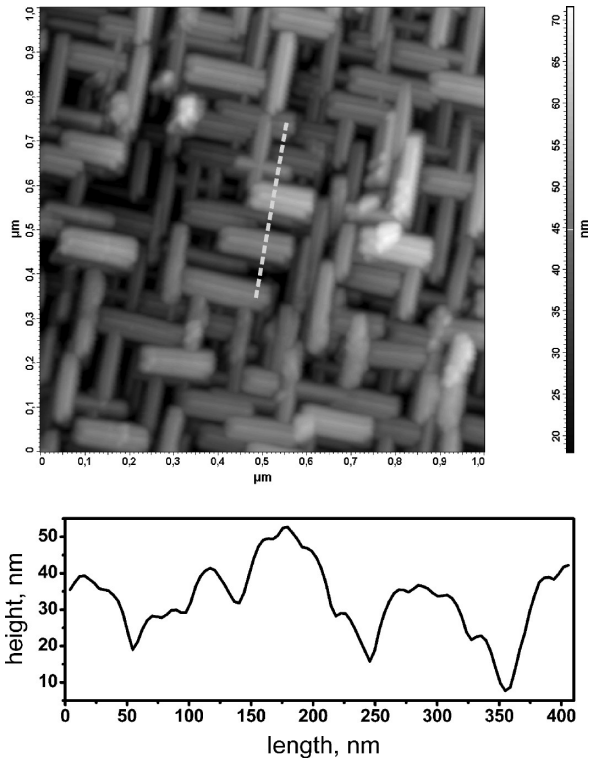

Figure 20. AFM image of rapidly grown (001) oriented SrF_2 film on *r*-sapphire with nanogrid structure and section profile of the image along the selected line.

system. The similar surface morphology was also observed in CaF_2 films deposited with rates under 2 Å/s.

The increase in the film growth rate led to coalescence of single (001) oriented crystallites along the fluorite *c*-axis. The surface of (001) oriented films of both CaF_2 and SrF_2 on *r*-sapphire deposited with the rates of 2−3 Å/s consists of submicrometer-sized formations (Figure 18a, shown is the micrograph for SrF_2 film on *r*-sapphire). A similar observation was made on 400 nm thick CaF_2 on (001) Si films grown at 550 °C by MBE.[52] A cross-section micrograph of our films (Figure 18b) shows they have columnar structure, with each column being comprised by numerous small (001) oriented crystallites joined with each other by their upper and lower planes (depicted schematically on Figure 16C). The lateral faces of these crystallites are, as it can be predicted from above said, (111) facets that give the columns a characteristic shape (see inset of Figure 18b). The column diameter was about 30−50 nm for CaF_2 and up to 120−160 nm for SrF_2 films.

However, the most remarkable and exciting was the third, not predictable, type of (001) oriented film morphology observed in the present study for CaF_2 and SrF_2 films on all used substrates deposited with rates > 3.5 Å/s. The surface of these films is comprised by numerous elongated crystallites intersecting at right angle to each other forming a single three-dimensional grid (Figure 19, shown is the micrograph of SrF_2 film on *r*-sapphire). Each certain crystallite represents a well-shaped rectangular-based bar, approximately 100−200 nm long and 30−50 nm wide. The longitudinal growth of the bars occurs along the [110] and [1$\bar{1}$0] axes of the fluoride. Using high-resolution AFM imaging techniques, we could visualize the fine structure of the bars, indicating the presence of fine hip rooflike (111)-faceted features on their top (Figure 20). The feature height of just several nanometers corresponds to less than 10 fluoride unit cells. This remarkable structure originates from in-plane coalescence of single (001) oriented crystallites driven by the minimization of film surface energy because of a decrease in intercrystallite interface surface. The coalescence occurs between the base edges of pyramidal crystallites providing the nanobars growth along the [110] and [1$\bar{1}$0] fluoride directions (see Figure 16D). The surface roughness R_s of such a nanogrid structure is found to be about 8 nm over a 1 × 1 μm^2 AFM scan.

To the best of our knowledge, there are very few recent works where similar well-ordered nanostructures were observed. Among them is the "nanofence" structure reported for MgO films grown by colaser ablation of MgO and Ni catalyst on $SrTiO_3$ substrates at high temperature.[62] However, there exist fundamental differences between this structure and the one reported in the present paper. MgO has a rock salt structure and the exposure of (100) surface in its crystal is mostly favorable from the energetic point of view.[58] It allows us to expect the possibility of MgO growth in the form of nanobelts, which is absolutely not the case for CaF_2/SrF_2, because of totally different energetic characteristics of their crystal surfaces, which in our case manifest themselves in facetting the top of the bars with (111) planes. Moreover, our synthesis procedure enables the growth of structured nanobars array without any additional components including catalyst and at low temperatures. The alike quasi-2D nanostructure was also reported for very thin (< 2 monolayers) films of alkaline-earth fluorides grown by MBE on Si (001) at 750−770 °C.[30,63] In contrast to these films, our samples had a highly developed three-dimensional structure that did not coalesce when increasing the film thickness and were obtained at significantly lower temperatures, which is an obvious advantage. At last, similar structures of high-T CeO_2 films obtained at 1000 or 745 °C on (001) yttria-stabilized zirconia or *r*-sapphire, correspondingly, have been reported.[64,65] The explanation for their formation[65] as being due to low deposition temperature and corresponding low mobility of CeO_2 adatoms and nuclei at this *T* does not contradict our results that clearly show it is the high growth rate that induces such film morphology.

Surface Texture. Particular attention was also paid to crystalline perfection and orientation of the film surface, which can serve as an ordered nanotemplate for oriented growth of the subsequent film. EBSD study of the thin surface layer (approximately 10 nm thick) of *c*-oriented

(62) Wee, S. H.; Goyal, A.; More, K. L.; Specht, E. *Nanotechnology* **2009**, *20*, 215608.
(63) Pasquali, L.; Suturin, S. M.; Kaveev, A. K.; Ulin, V. P.; Sokolov, N. S.; Doyle, B. P.; Nannarone, S. *Phys. Rev. B* **2007**, *75*, 075403.
(64) Costa-Nunes, O.; Gorte, R. J.; Vohs, J. M. *J. Mater. Chem.* **2005**, *15*, 1520.
(65) Murugesan, M.; Obara, H.; Nakagawa, Y.; Yamasaki, H.; Kosaka, S. *J. Cryst. Growth* **2007**, *304*, 118.

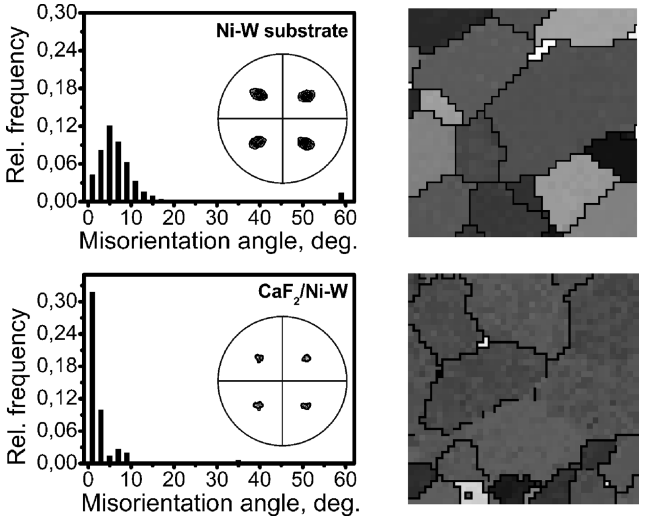

Figure 21. EBSD data for Ni−W tape and CaF_2 film on it: profiles of grain misorientation angles with pole figures for (111) reflection and corresponding orientation maps ($80 \times 80\ \mu m^2$). Misorientation angle is reflected by pixel color depth (full range of grayscale palette covers the misorientation angles from 0 to 60°).

fluoride films demonstrated its perfect crystallinity and sharp in-plane orientation. EBSD hit rates (i.e., the percentage of indexed diffraction patterns recorded during the analysis) were 94−100% for samples on single-crystal substrates and somewhat lower for those on Ni−W, which is quite expectable because the metal substrate surface contains numerous defects (e.g., grain boundaries) that complicate film epitaxy on this surface. The grain misorientation level was as well substantially predetermined by the substrate nature: it varied from almost 0° for films on single-crystal substrates to several degrees for films on Ni−W tapes, which is expectable for films on well-textured but still polycrystalline substrate. However, the in-plane grains alignment was usually better for the films than for metal substrates due to the heteroepitaxy (Figure 21, shown are the data for CaF_2 film on Ni−W).

Conclusions

We have demonstrated a simple and reproducible method to grow epitaxial thin films of CaF_2 and SrF_2 on different single crystalline and (for the first time) polycrystalline metal substrates by MOCVD using a separate fluorine source. Some of the films required an additional postdeposition annealing to form the epitaxial (00*l*) oriented layer. The optimal annealing temperatures were found to be different for CaF_2 and SrF_2. For both materials the influence of substrate type, deposition rate, and film thickness on its orientation was analyzed. It was shown that slow deposition of SrF_2 on *r*-sapphire results in (111) oriented films, while increase of the growth rate as well as improving lattice match with the substrate (e.g., change of the substrate to MgO or Ni−W or change the film material to CaF_2 having a smaller lattice parameter) enable the formation of *c*-axial orientation in the fluoride layer. Depending on the films orientation and growth rate, their surface morphology was shown to be different: rather smooth for (111) oriented films, and much rougher for (001) oriented. The explanation for this phenomenon as well as for the observed surface morphologies is given in the context of minimization of the system total surface energy. The obtained films demonstrated perfect out- and in-plane orientation both in the bulk of film and in thin surface layer. Besides, certain deposition conditions were found under which the films grown have a unique three-dimensional ordered nanogrid structure, which was observed for the first time in such films. The coexistence of this remarkable structure and perfect texture in the same layer makes such films very promising templates for epitaxial growth of numerous nanodevices or structurally matched films of various compositions.

Acknowledgment. The authors are sincerely grateful to V.S. Kulikauskas (SINP MSU, Moscow), R.Yu. Muydinov and O. Stadel (IOT, TU Braunschweig, Germany) for their help with sample analyses. This work was financially supported by SuperOx Company (Russia) and INTAS (Grant YSF-06-1000014-6499).